Journal of the European Ceramic Society 41 (2021) 3292–3302

Contents lists available at ScienceDirect

Journal of the European Ceramic Society

journal homepage: www.elsevier.com/locate/jeurceramsoc

Influence of DVB as linker molecule on the micropore formation in polymer-derived SiCN ceramics

C. Drechsel [a], H. Peterlik [b], C. Gierl-Mayer [a], M. Stöger-Pollach [c], T. Konegger [a,*]

[a] TU Wien, Institute of Chemical Technologies and Analytics, 1060, Vienna, Austria
[b] University of Vienna, Faculty of Physics, 1090, Vienna, Austria
[c] TU Wien, University Service Center for Transmission Electron Microscopy (USTEM), 1040, Vienna, Austria

ARTICLE INFO

Keywords:
Polymer-derived ceramics
Polysilazane
Preceramic polymers
Pyrolytic conversion
Microporosity

ABSTRACT

In this work, the formation of transient microporosity during the polymer-to-ceramic conversion in polymer-derived ceramics was studied using a commercially available poly(vinyl)silazane precursor which was modified with divinylbenzene (DVB) as linker molecule during crosslinking. After pyrolysis treatments between 400 and 700 °C, the resulting materials not only showed distinct changes in elemental composition and structural features upon introduction of the linker molecule, but also a shift in micropore size, e.g. shifting from 0.84 nm to 0.70 nm after pyrolysis at 600 °C. Due to hindrance of transamination reactions in the low-temperature region, the nitrogen content in linker-containing samples was significantly higher, leading to a different composition of micropore-forming entities and, in case of the system studied, to smaller pores. These findings are a first step towards the clarification of the mechanisms leading to the pore formation in PDCs during pyrolytic conversion, which is essential for their use in prospective applications.

1. Introduction

Since environmental challenges have become more urgent and a central topic of public awareness in the last years, the need for more sustainable, energy-saving processes as well as the use of renewable energy have raised increasing public and industrial interest. A particular focus has been set on the development of new and well-tailored separation and catalysis processes, accompanied by increasing technological requirements placed on the materials used. Ceramics fulfil these requirements to a great extent, exhibiting superior chemical and high-temperature mechanical properties compared to conventionally used polymers or metals. Porous ceramics are promising candidates for applications as membrane or catalyst supports, where polymer- or metal-based structures are unsuitable due to the process conditions such as high temperature or harsh chemical environments. Especially in separation processes employing porous membranes, it is crucial to have a well-defined pore size in order to guarantee reliable and satisfactory selectivity. For an application in gas separation, the pore size has to be below 2 nm (and therefore - per IUPAC definition – microporous [1]) to move from the low-selectivity Knudsen diffusion regime to micropore diffusion, yielding higher selectivities [2].

To optimize the high temperature properties, the materials of choice are non-oxide ceramics like SiC and Si_3N_4, which can be deposited e.g. by chemical vapour deposition (CVD). Another route to non-oxide ceramics is the use of preceramic polymers, which are converted to so-called polymer-derived ceramics (PDCs) after the shaping process. Typically, silicon-based polymers are used as precursors, examples including polysiloxanes, polysilazanes, or polycarbosilanes. The composition of the resulting ceramics is primarily affected by the precursor structure and composition, as well as by the pyrolysis conditions during the polymer-to-ceramic conversion process. Since their emergence in the production of ceramic fibers as reported by Yajima et al. [3], polymer-derived ceramics have become a research field of great interest during the last decades [4–6]. PDCs exhibit several advantages when compared to traditional powder-based processing of ceramics, including higher flexibility in processing and shaping, high purity of the precursor materials, and relatively low processing temperatures. As a consequence, they have become the material of choice for special applications in a variety of fields [7–10]. Examples are the production of ceramic fibers and coatings [10–13], the application in micro-electro-mechanical systems (MEMS) [8,14–17], as well as the use of cellular PDCs in applications such as hot metal filtration, insulation, or catalyst support. [18–21].

An additional feature of this material class is the evolution of

* Corresponding author.
E-mail address: thomas.konegger@tuwien.ac.at (T. Konegger).

https://doi.org/10.1016/j.jeurceramsoc.2021.01.051
Received 28 September 2020; Received in revised form 9 January 2021; Accepted 26 January 2021
Available online 1 February 2021

microporosity under certain pyrolysis conditions, which opens up the field of an application as (hot) gas separation membrane [22–24]. This so-called transient porosity is usually present only at intermediate pyrolysis temperatures and varies in temperature range and volume depending on the structure and composition of the precursor [25–31]. Due to their excellent stability regarding temperature and harsh chemical environments, non-oxide ceramics in particular are of interest for many applications. A typical precursor for polymer-derived SiCN ceramics are poly(vinyl)silazanes. However, if treated in inert atmosphere, microporosity in poly(vinyl)silazane-derived ceramics collapses at temperatures around 700 °C, which has led to intensive investigations towards the stabilization of the micropore network at higher temperatures. Major work in this direction was done by Dismukes et al. [25], presenting several ways to retain microporosity even at higher pyrolysis temperatures, including the addition of micron-sized ceramic fillers, the use of ammonia as reactive atmosphere, the introduction of metals in form of a polysilazane-stabilized metal nanocolloid, or a polysilazane/metal-organic mixture. The obtained non-oxide ceramics retained their microporosity at temperatures of at least 700 °C with high specific surface areas and micropore volumes in the range of 0.2 cm^3/g. The most promising approaches of this work, the use of a reactive atmosphere and metal nanoparticles, were studied more intensively in later works. Ammonia leads to increased stability of the microporosity in many cases, reported e.g. by Bradley et al. [32] and Schitco et al. [29,30], who carried out studies dedicated to the use of ammonia as pyrolysis atmosphere. The introduction of metal particles or in-situ formation of metal clusters was further investigated and applied to a variety of metals [28,33–35].

For optimal adaption to different needs of various applications, it is necessary to have a well-defined and tailorable pore size, thus requiring a thorough understanding of the pore evolution mechanisms. Albeit several works have been carried out to clarify the decomposition behaviour of various precursors, the mechanisms leading towards transient pore structures are still not fully understood yet [36–41]. Various hypotheses have been made towards pore formation mechanisms, stating that the release of small gaseous species during the decomposition, combined with molecular rearrangements, leads to the formation of a (micro-)pore network [42]. Schitco et al. [29] also stated that micropore-forming entities could already be present in the precursor structure.

One of the model precursors studied by several groups is a commercially available poly(vinyl)silazane, which has already been investigated intensively with respect its pyrolysis behaviour and porosity evolution during pyrolysis [29–31]. This poly(vinyl)silazane yields amorphous silicon(oxy)carbonitrides with varying compositions depending on pyrolysis conditions and -atmosphere, which begin to crystallize at around 1400 °C. The pore size is around 0.8 nm up to pyrolysis temperatures of 600 °C, and the pores collapse at temperatures between 600 °C and 700 °C if an inert atmosphere is used [31].

The use of linker molecules is a straightforward method to modify the resulting structural and chemical composition of polymer-derived ceramics. Divinylbenzene (DVB) in particular has been commonly used as a crosslinking agent for preceramic polymers. With its two reactive vinyl groups, it can increase the molecular weight of preceramic polymers by reactions such as hydrosilylation at low temperatures. This consequently prevents the loss of volatile species during pyrolysis and increases the ceramic yield. [43] Also, it is a versatile tool to increase the carbon content of the resulting PDCs, which could be beneficial for prospective use in electrochemical applications. This is due to the formation of sp^2-carbon domains, which increase the electrical conductivity of the material. [44–47] The investigation of the influence of the carbon content on the thermal stability and crystallization temperature of PDCs benefits from the straightforward adjustment of the carbon content by addition of DVB, as opposed to more complex procedures such as variation of the precursor [48]. In a related work, Chen et al. [49] described the preparation of SiCN-carbon nanocomposites by a direct reaction between poly(vinyl)silazane and DVB followed by pyrolytic conversion at 1200 °C. Carbon nanodomains in the final material were generated by a two-step cross-linking treatment, leading to phase separation of DVB nanoclusters at 70 °C before subsequent cross-linking of the poly(vinyl)silazane at 120 °C.

The objective of this work is the identification of reactions and mechanisms leading to the formation of transient pores in poly(vinyl)silazane upon introduction of linker molecules, hereby contributing to a deeper understanding of the generation of porosity in polymer-derived ceramics in general. Furthermore, from a technological point of view, it is our aim to eventually correlate the decomposition behaviour with both pore evolution and resulting pore size. With respect to these objectives, a straightforward modification of the commercially available poly(vinyl)silazane is carried out by adding a well-known linker molecule, divinylbenzene (DVB), during the crosslinking step and thereby integrating it in the resulting crosslinked network. This linker molecule was added in an overstoichiometric amount, leading to a separation of the actual precursor oligomers, hence decreasing the degree of direct interaction with each other. In contrast to previous works focusing on nanocomposite fabrication (e.g. [49]), where intermediate heat treatment steps were used to promote premature polymerization and, hence, phase separation of DVB, in the present work, integration of DVB into the network was achieved by a single-step cross-linking treatment at 120 °C. To investigate the effect without superposition with other factors such as a reactive pyrolysis atmosphere, the experiments were carried out in a relatively low temperature range, where porosity can still be observed in the original material. To evaluate a potential increase in thermal stability of the resulting (micro-)porosity, a further test was carried out a temperature above the critical pyrolysis temperature of the unaltered material. The effect on the pyrolysis behaviour in combination with the pore characteristics of the resulting ceramics can give insight in the correlation between decomposition and pore formation. Although the specific materials produced in this study might not be directly feasible for high-temperature applications, they will help to identify the crucial parameters during the polymer-ceramic-conversion responsible for and affecting the micropore formation. By contributing towards a deeper understanding of these fundamental processes, we expect a definite impact on the applicability of this class of materials with regard to prospective applications in separation or catalysis.

2. Experimental

A commercially available liquid poly(vinyl)silazane (*PSZ*, Durazane 1800, DurXtreme GmbH) was used as primary precursor compound. Due to its sensitivity towards hydrolysis, PSZ was handled under nitrogen atmosphere, and was thoroughly degassed in vacuum before each use to remove decomposition products. As linker molecule, divinylbenzene (*DVB*, Sigma Aldrich, 80 % isomer mixture) was used, which was distilled freshly before application. Samples with a molar ratio of 0.8 equ. of the linker molecule DVB in relation to PSZ (monomer unit) were crosslinked by a hydrosilylation mechanism using 100 ppm of Karstedts catalyst (Sigma Aldrich, Platinum(0)-1,3-divinyl-1,1,3,3-tetramethyldisiloxane complex solution, in xylene, ~2% Pt). This DVB/PSZ ratio corresponds to twice as many vinyl groups provided by DVB than Si-H groups provided by PSZ, leading to an overstoichiometric amount of DVB. The three compounds were mixed under nitrogen atmosphere (1.0 g of PSZ, 1.6 g of DVB, 5 µl of catalyst solution, for a typical sample amount of 2.6 g) and then crosslinked at 120 °C for 12 h under flowing nitrogen (0.35 l/min; purity > 99.999 %). The starting compounds as well as the resulting crosslinked network are schematically displayed in Fig. 1, taking into account that DVB molecules can be expected to also react with each other via polyaddition. TGA-MS measurements were carried out up to 1000 °C under nitrogen atmosphere (heating rate of 10 K/min) using a Netzsch STA 449 C (Jupiter) coupled to a quadrupole mass spectrometer (Netzsch QMS 403 C, Aëolos). Additionally, samples were pyrolyzed in a tube furnace (Carbolite HZS

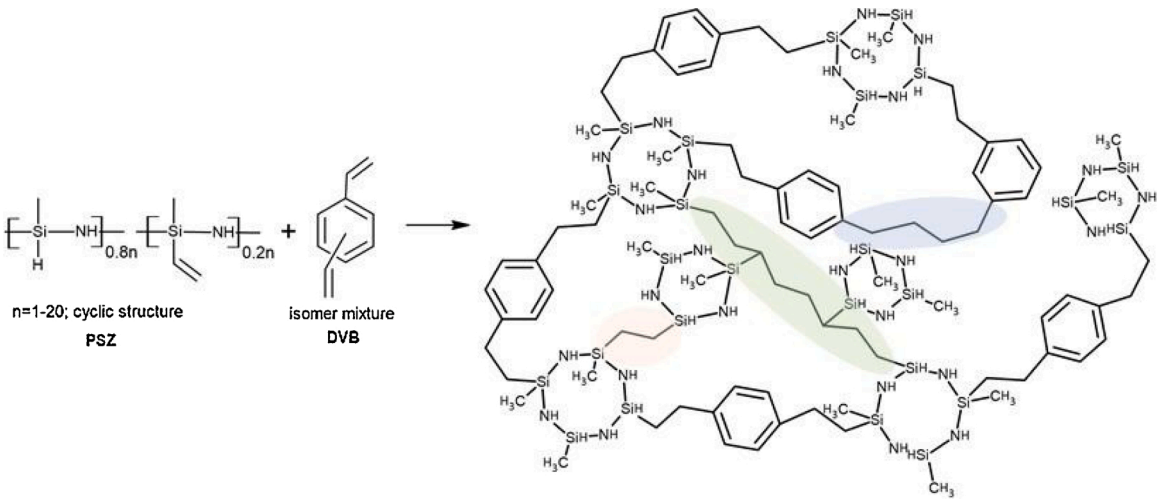

Fig. 1. Simplified reaction scheme of the hydrosilylation reaction between PSZ and DVB, with alternative reactions highlighted in different colors: polyaddition of DVB molecules (blue), polyaddition of PSZ molecules (green), and hydrosilylation between PSZ molecules (orange) (For interpretation of the references to colour in this figure legend, the reader is referred to the web version of this article).

12/600) at temperatures from 400 °C to 700 °C, using a heating rate of 3 K/min up to 300 °C and 1 K/min up to the maximum temperature, at which they were held for 4 h followed by cooling at a rate of 3 K/min. The prepared samples without linker are named *PSZ*, those with DVB as linker are named *2DVB*, where applicable with the pyrolysis temperature added.

The crosslinked samples were first characterized regarding their elemental composition. Oxygen and nitrogen content were determined using an O/N determinator (Leco TC400), the powdered samples being placed in tin capsules. The carbon content was measured using a carbon determinator (Leco C230), using alumina crucibles with alumina lids and Lecocel as ignition accelerator. In addition to elemental analysis, ATR-IR investigations were conducted using a Tensor 37 instrument (Bruker). The samples were finely ground and measured immediately. The spectra were then normalized with regard to the $Si-CH_3$ signal (from 1230 to 1300 cm^{-1}) to enable comparability of the different samples.

The pyrolyzed samples were characterized in a similar manner. In addition to elemental analysis and IR spectroscopy, the pore structure was investigated using two distinct methods, gas physisorption and small angle X-ray scattering (SAXS). The physisorption experiments were carried out at 77 K, using nitrogen as adsorptive (ASAP2020, Micromeritics). The samples were finely ground and transferred to the sample tubes inside a glovebox. The samples were then degassed overnight at 250 °C in vacuum. Furthermore, a degas step at the analysis port was performed prior to the actual analysis. The analysis was carried out in the pressure range from $5 \cdot 10^{-6}$ bar to saturation pressure for the adsorption branch and back down to 0.2 bar for the desorption branch of the isotherm. The specific surface area was estimated using the Brunauer-Emmett-Teller method (BET) with five values located in the linear range of the isotherm. The pore size distribution was determined using a non-local density functional theory (NLDFT) model (model: Carbon-N_2, 2D-NLDFT Heterogeneous Surface, SAIEUS software package). As second method for the evaluation of the pore characteristics, SAXS investigations were carried out, using a Bruker Nanostar equipped with a microfocus source (Incoatec High Brilliance, Germany) and a 2D position sensitive detector (Vantec 2000, Bruker AXS). The samples were placed between two Scotch tapes. Collected X-ray data were radially integrated and background corrected to obtain scattering intensities in dependence on the scattering vector q. For evaluation, the same model as in a previous work [31] was used, describing slightly agglomerated pores with a unified fit function [50] and a structure factor from a hard sphere model [51].

For selected samples, further characterizations concerning structural features were carried out using solid state NMR spectroscopy. Solid-state nuclear magnetic resonance spectra were recorded with a Bruker spectrometer model AVANCE 300 equipped with a 4 mm broadband probe head ($^{13}C = 75.40$ MHz, $^{29}Si = 59.57$ MHz). All NMR measurements were conducted in CP/MAS mode with a rotational speed of 4 kHz.

Raman investigations were carried out using a WITec alpha 300RSA + Raman microscope. Raw Raman data were processed by Savitzky-Golay smoothing and baseline correction. Where applicable, Lorentz fits were applied for further data interpretation.

A transmission electron microscope (TEM; FEI TECNAI F20) was used for high-resolution imaging. Electron energy loss spectrometry (EELS) was measured in scanning mode of the TEM by focusing the electron beam to a diameter of 10 Ångström. In every pixel an EELS spectrum was acquired measuring the Carbon-K edge at 284 eV energy loss. The intensity in the range from 284−294 eV was used for mapping the relative carbon concentration. For this purpose, the EELS-map was divided by a thickness map, as reported by Hofer et al. [52].

3. Results and discussion

The main focus points of this work are (i) the description of the reaction between DVB and PSZ, (ii) the general thermal decomposition behaviour of PSZ both in absence and presence of DVB, (iii) the effect of the introduction of DVB on the properties of the resulting PSZ-derived ceramics with respect to elemental composition and chemical structure, and (iv) the effect of DVB introduction on porosity with a focus on the micropore range. These points will be discussed in the subsequent sections.

3.1. Preparation of DVB-linked PSZ

The initial reaction between DVB and PSZ was carried out at 120 °C by a hydrosilylation mechanism using Karstedts catalyst. By using a catalyst-assisted single-step heat-treatment process, a deliberate premature phase-separation of DVB nanoclusters before cross-linking of PSZ, described e.g. by Chen et al. [49], was avoided.

During the hydrosilylation reaction, which is schematically displayed in Fig. 1, Si-H groups react with double bonds, forming aliphatic groups attached to the silicon atom. Therefore, a significant decrease of the Si-H related signal should be visible in IR. The respective spectra of PSZ and 2DVB after cross-linking are displayed in Fig. 2. Although an excess of DVB was used for the 2DVB sample, the intensity of the Si-H

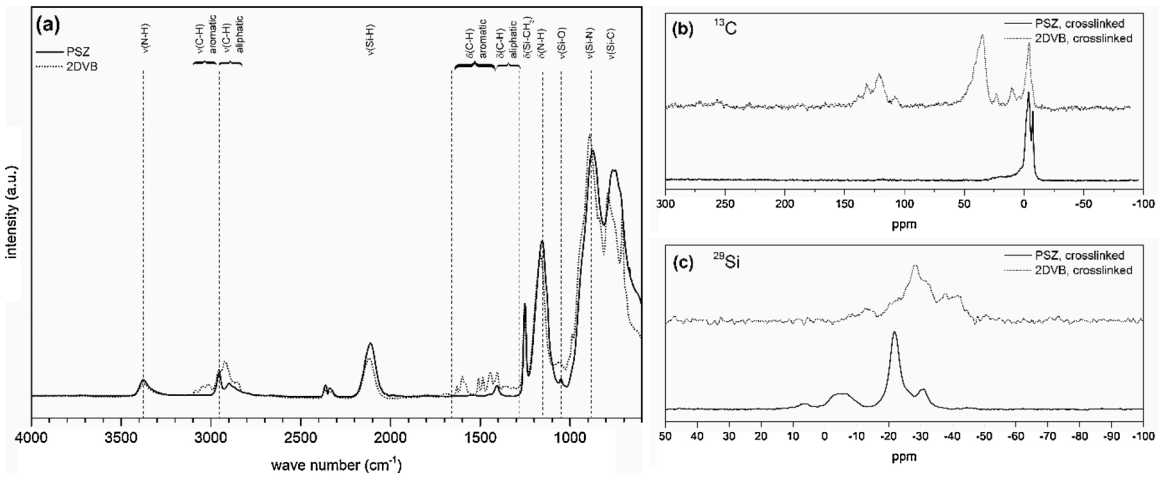

Fig. 2. FTIR (a) and solid-state NMR results of PSZ and 2DVB materials after cross-linking, ^{13}C (b), ^{29}Si (c).

band at 2100 cm^{-1} only decreases by approximately one third, which is in accordance with the findings by Liu et al. [44], who also observed that for this specific precursor, even an overstoichiometric amount of DVB does not lead to a complete consumption of the Si-H groups. The hydrosilylation reaction appears to be sterically hindered, and even an excess of DVB cannot achieve a complete reaction of the Si-H groups. Bands attributed to DVB can be found in the region of aromatic C—H vibrations (~3000–3100 cm^{-1} and from 1400–1650 cm^{-1}). The increased intensity of the aliphatic C—H bands at ~ 2900 cm^{-1} indicates the reaction of the double bonds of both DVB and PSZ during hydrosilylation or polyaddition in the crosslinking process.

To further investigate the bonds generated during the crosslinking process, solid-state NMR spectra were recorded, which are shown in Fig. 2b and c. The comparison of the ^{13}C spectra shows one main signal for PSZ around 0 ppm, which is also present in the 2DVB sample. This signal corresponds to the Si-$\mathbf{C}H_3$ groups. For 2DVB, there are two additional signals at chemical shifts of 40 ppm and 135 ppm, respectively. The latter one originates from the aromatic ring sp^2 carbon, whereas the one around 40 ppm is caused by the sp^3 carbon in the aliphatic chains generated by opening of double bonds during hydrosilylation or polyaddition. This observation corresponds well with the IR spectra. Three signals were found for PSZ in the ^{29}Si NMR spectrum, with the main one at -17 to -25 ppm originating from typical Si-environment in the pure poly(vinyl)silazane -$SiCH_3H$-NH- [23]. The smaller peak at 0 to -10 ppm, which, according to Gérardin et al. [53] and Riedel et al. [39], can be attributed to $SiC(sp^3)_2N_2$, could be due to

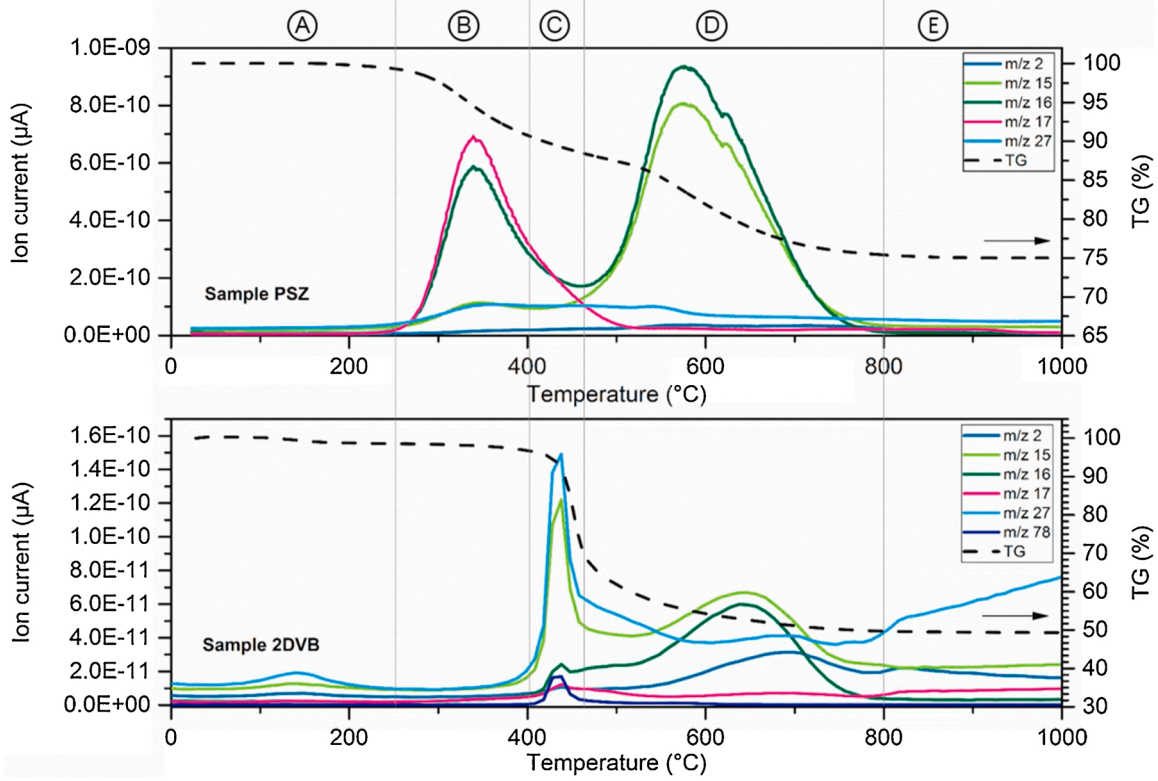

Fig. 3. TGA curves and corresponding m/z values detected by MS for PSZ (top) and 2DVB (bottom) up to 1000 °C; Region A: Distillation of volatile species, B: Ongoing crosslinking, C: Partial decomposition of DVB, D and E: Polymer-to-ceramic conversion. $m/z = 2$: hydrogen, $m/z = 15$, 16: C_1-species, methane; $m/z = 17$: ammonia, $m/z = 27$: C_2-species, ethane; $m/z = 78$: benzene.

the double bonds in the vinyl groups opening up during crosslinking. All signals of 2DVB are shifted to more negative values, showing the different chemical environment of the Si atoms. The main signal is now around -25 ppm, and most likely caused by the newly generated bonds between DVB and PSZ during hyrosilylation. The shoulder around -20 ppm is comparable to the main signal of PSZ, showing the presence of unreacted Si-H groups and therefore the original -$SiCH_3H$-NH- groups. The NMR investigations confirm the results found by IR spectroscopy. In addition, they show that there was not only phase separation happening between DVB and PSZ, since there are also major differences found in the Si spectra indicating direct interactions between the two materials.

3.2. Decomposition behavior

Using thermogravimetric analysis combined with mass spectroscopy, the reactions during pyrolytic conversion of crosslinked PSZ and 2DVB were monitored in order to evaluate the effect of DVB on the general decomposition behaviour. As shown in Fig. 3, the mass change behaviour and evolving gas species differ drastically, especially up to temperatures of 500 °C. In the lowest temperature region (A), there is typically a competition between evaporation and crosslinking of low molecular weight compounds. As samples previously crosslinked were investigated here, no signals should be detected in this temperature range, which is indeed the case for PSZ. For 2DVB, several signals were found at temperatures below 200 °C, which can be attributed to fragments of DVB. This indicates an incomplete reaction of DVB during the crosslinking step, resulting in a release of DVB-related gas species as temperatures approach the boiling point of DVB (*bp* =195 °C). More conclusive differences are found in regions B and C, where further crosslinking of the samples takes place. According to literature reports, the primary crosslinking mechanisms here are hydrosilylation and transamination reactions (Fig. 4, [37]). Hydrosilylation occurs without mass loss and release of decomposition products and therefore cannot be observed by TGA-MS; in contrast, transamination reactions lead to chain scission and formation of new connections between the oligomers under release of ammonia, which can be detected by MS ($m/z = 17$). In case of PSZ, ammonia is indeed the main signal that is found up to a temperature of 500 °C. Simultaneously, the breaking of the chains formed during crosslinking can be observed by detection of fragments at $m/z = 27$ (C_2 species). In contrast, 2DVB shows neither mass change nor a significant release of gaseous species between 200 °C and 400 °C, where the ammonia signal is already declining for PSZ. These findings lead to the assumption that the presence of an overstoichiometric amount of DVB prevents PSZ oligomers from interacting with each other, thus hindering transamination reactions. Between 400 °C and 500 °C (region C), several sharp and simultaneous signals are detected for 2DVB, showing partial release of DVB, observed e.g. by ring-containing fragments (exemplarily shown by signals at $m/z = 78$), and breaking of alkyl chains that were formed during the crosslinking process ($m/z = 15$, 16, 27). The evolution of ammonia starts with a slight delay to the decomposition of DVB. Since the absolute values of the detected ion currents cannot be directly compared between measurements, in contrast to the ratio between the signals, the ammonia formation is set in relation to another signal, e.g. the methane formation ($m/z = 16$) in region D. By doing this, it can be seen that ammonia formation is not only delayed, but also takes place to a much smaller extent, which is in accordance with the assumption that the presence of DVB in the precursor oligomers hinders transamination reactions. As a consequence, DVB has to be partially decomposed before PSZ oligomers can interact with each other. The same trend is found for the actual polymer-to-ceramic conversion, which takes place mainly in region D (up to 800 °C), and is followed by further rearrangements under release of hydrogen and small carbon containing compounds, in case of 2DVB up to 1000 °C (region E). Mechanisms for the decomposition reactions have been suggested by Bahloul et al. [37], accompanied by the release of small gaseous species, mainly methane ($m/z = 15$, 16) and hydrogen ($m/z = 2$). These reactions are shifted to higher temperatures in case of 2DVB.

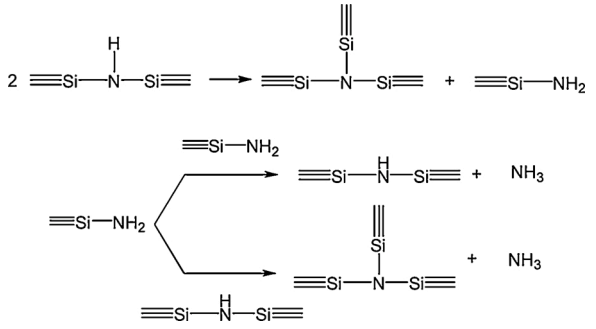

Fig. 4. Reaction scheme of transamination reactions showing the ammonia formation; after [37].

3.3. Composition and structural features

Based on the initial decomposition studies, the crosslinked samples as well as the heat-treated samples were further characterized. By investigating the elemental composition, the integration of the DVB in the network was monitored, and the changes in composition during ongoing pyrolysis were observed. In order to obtain information about the bonds present and changes with increasing pyrolysis temperature, as well as to evaluate the completion of the hydrosilylation reaction, infrared spectra were recorded for the crosslinked samples and the samples after the respective heat treatment steps. Solid-state NMR measurements were conducted for the samples pyrolyzed at 600 °C in order to further clarify structure and chemical surroundings in the pyrolyzed stage.

3.3.1. Elemental composition

The elemental compositions of the crosslinked as well as the pyrolyzed samples are summarized in Table 1. The increase in carbon content, together with a decrease in nitrogen and silicon content, shows that DVB was indeed integrated in the crosslinked network. This can be illustrated even better by comparing the experimental composition of crosslinked 2DVB with the theoretically calculated composition. Apart from the oxygen content (which is not taken into account when calculating the theoretical composition), the compositions correspond very well to their expected values, indicating a complete integration of the DVB into the crosslinked sample. The pyrolyzed samples have a comparable oxygen content due to the presence of oxygen in the as-received precursor, a slight increase caused by the handling procedure, especially in case of the DVB samples. For the pyrolyzed samples, the carbon content is increased for the DVB containing samples, illustrated by the Si (+H)/C ratio (derived from the composition in wt%, Fig. 5), which is

Table 1
Sample composition of crosslinked PSZ, 2DVB and the pyrolyzed samples, with measured oxygen, nitrogen, and carbon contents; the remainder to 100 % is listed as silicon and hydrogen content.

	O (wt%)	N (wt%)	C (wt%)	Si+H (wt%)
PSZ	5 ± 1	19 ± 2	25 ± 1	51 ± 6
2DVB	4 ± 1	9 ± 1	68 ± 5	16 ± 6
$2DVB_{th}$	0	8.5	66.5	25
PSZ400 °C	3 ± 1	19 ± 1	29 ± 1	49 ± 1
PSZ500 °C	3 ± 1	15 ± 1	26 ± 1	56 ± 1
PSZ600 °C	2 ± 1	12 ± 3	19 ± 1	67 ± 5
PSZ700 °C	2 ± 1	15 ± 1	20 ± 3	63 ± 4
2DVB400 °C	4 ± 1	10 ± 1	53 ± 2	33 ± 3
2DVB500 °C	2 ± 1	12 ± 2	46 ± 3	40 ± 5
2DVB600 °C	7 ± 1	14 ± 2	43 ± 3	36 ± 6
2DVB700 °C	6 ± 1	14 ± 2	43 ± 3	37 ± 4

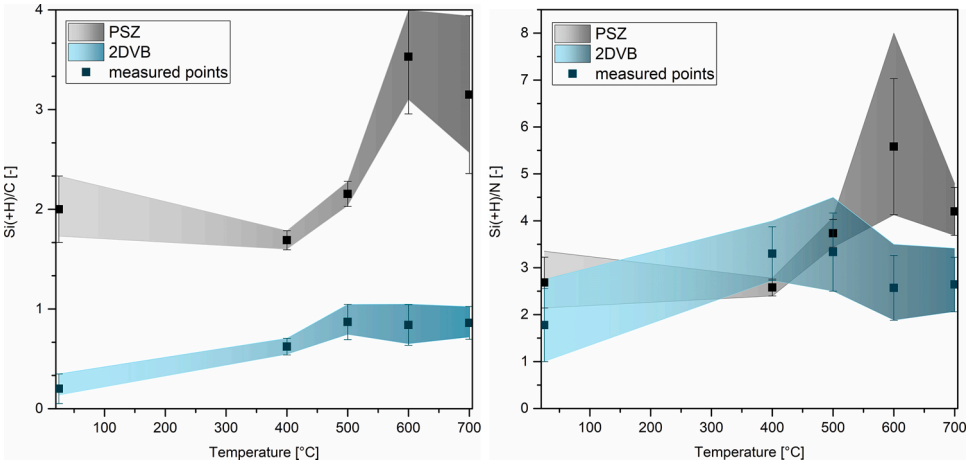

Fig. 5. Si(+H)/C ratio (left) and Si(+H)/N ratio (right) calculated from the elemental composition (mass-based) for PSZ and 2DVB in the crosslinked stage and after pyrolysis at 400, 500, 600 and 700 °C.

always clearly higher than in case of pure PSZ. This indicates that DVB is not completely removed during pyrolysis, even though signals attributable to DVB and its fragments and a higher mass loss than for pure PSZ were observed by TGA-MS. The nitrogen content slightly decreases during pyrolysis in case of pure PSZ, while it its slightly increasing in case of 2DVB. To ensure that this phenomenon is not merely a consequence of the decomposition of DVB, the mass-based Si(+H)/N ratio (from the composition in wt%) was calculated. In the initial material, this value should be equal to 2, as the molar ratio of silicon to nitrogen is 1 in the polysilazane backbone. While the ratio increases for PSZ with increasing temperature, corresponding to a reduced nitrogen content in relation to the silicon that is present, it stays almost constant for 2DVB. This indicates that reactions leading to nitrogen loss are hindered by the presence of DVB, again being in accordance with the findings of the TGA-MS investigations, where transamination reactions were found to occur at a smaller extent, thus retaining more nitrogen in the decomposition products.

3.3.2. *Infrared spectroscopy*

The recorded spectra of PSZ and 2DVB specimens in cross-linked and pyrolyzed state are displayed in Fig. 6. The spectra of the crosslinked samples were already discussed in detail in Section 3.1 (Fig. 2). Although DVB was used in an overstoichiometric amount, the Si-H groups were not fully consumed. Nevertheless, according to the elemental analysis, the full amount of DVB is present in the sample, indicating that DVB molecules have indeed reacted with each other. The formation of larger C-domains thus causes an even higher separation of the PSZ oligomers. The benzene ring of DVB can be seen in different areas of the spectra, e.g. at around 1550–1620 cm^{-1} and 3000–3100 cm^{-1} due to C—Hvibrations, and at 1650–2000 cm^{-1} due to the C—H bending ("benzene-fingers"). In addition, there is also a rise in aliphatic C—H signals for the 2DVB specimens, which is due to the opening of the double bonds during the reaction. These signals can be observed between 1400 and 1530 cm^{-1}. In case of the pyrolyzed samples, the Si—H signal is only present up to temperatures of 400 °C (cf. 500 °C for PSZ), which indicates a higher degree of hydrosilylation

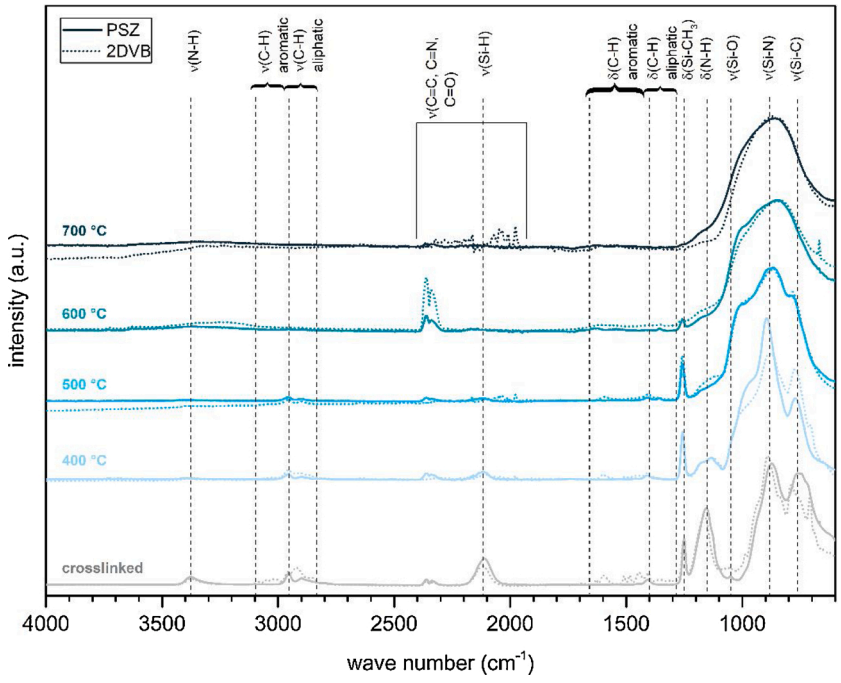

Fig. 6. ATR-IR spectra of PSZ and 2DVB after crosslinking as well as for pyrolysis temperatures from 400 °C to 700 °C.

reactions at elevated temperatures due to the presence of an increased amount of unsaturated bonds. On the other hand, aromatic signals can be found at all pyrolysis temperatures in case of 2DVB. In addition, the broad signal of O—H stretching at 3300 cm^{-1} can be observed, showing the slightly higher degree of oxidation of the samples containing DVB. Also, signals around 2000−2300 cm^{-1} appear at temperatures of 400 °C, which can be attributed to trivalent C≡C or C≡N moieties. The shoulder of the main signal is located at 1180 cm^{-1}, where N—H vibrations were found. Additionally, the shape of the main signal changes and is shifted to higher wave numbers. Since this signal is in the wave number range of Si—N and Si—C vibrations, the change of the shape shows a different ratio of Si-N to Si-C bonds.

3.3.3. Solid state NMR

^{13}C and ^{29} Si solid-state NMR spectra were recorded for the samples pyrolyzed at 600 °C (Fig. 7). When looking at the ^{13}C NMR spectrum for PSZ, the main signal at around 0 ppm results from Si-C bonds of carbon (sp^3) in a silicon network. In addition, there is a broad signal at 137 ppm, typically caused by sp^2 carbon. The signals at 85 ppm and 189 ppm are most likely spinning sidebands (marked by an asterisk) caused by chemical shift anisotropy [30]. The 2DVB sample shows the same peaks, but with different intensities – the sp^2 carbon signal is present at a higher intensity, due to DVB remaining in the sample and a free carbon phase formed by DVB domains, respectively. The ^{29}Si spectrum of PSZ shows a very broad peak that consists of several overlapping peaks, which were deconvoluted using a Gaussian approximation. Three maxima were found at -8, -24 and -37 ppm, with decreasing intensity in this order. According to the TGA-MS results shown above, hydrogen evolution can be observed up to 900 °C, indicating that there is still hydrogen present in the material at 600 °C. Hence, the material most likely consists of mixed Si-C-N-O-H tetrahedra. Dismukes at al. [25] observed a similar spectrum with a maximum at -21 ppm and shoulders at -7 and -40 ppm, which was attributed to silicon in carbon or a mixed carbon-nitrogen environment. Schitco et al. [30] investigated the same base material as used in this study, but applied a higher temperature for pyrolysis (750 °C), resulting in a spectrum similar in shape but shifted to more negative values. Literature provides chemical shifts for SiN_4 and SiC_4 tetrahedra, as well as several mixed tetrahedra. Pure Si_3N_4 is built by SiN_4 tetrahedra that appear at -47 ppm (±1 ppm), while SiC_4 tetrahedra appear from -10 to -25 ppm [30,54], or even up to 0 ppm, according to Williams et al. [26] According to Kenneth et al. [54], $SiCN_3$ tetrahedra, SiC_2N_2 tetrahedra, and SiC_3N tetrahedra range from -35 to -25 ppm, from -25 to 0 ppm, and from 0 to 30 ppm, respectively. According to Williams et al. [26], $SiHC_3$ and SiH_2C_2 moieties can be found at -17 ppm and-38 ppm, respectively, and SiH_3C tetrahedra are located at around -67 ppm. Mixed Si-H-C-N moieties are likely to be present, too, which are located at -19 ppm for $SiHC_2N$ and at -24 ppm for $SiHCN_2$ [55]. For the spectrum of PSZ, the deconvoluted peaks (-8, -24, and -37 ppm, as mentioned above) can thus be described best by the presence of SiC_2N_2, $SiHCN_2$ and $SiCN_3/SiH_2C_2$ tetrahedra, taking into account the chemical shifts found in literature. For 2DVB, the peak in the ^{29}Si spectrum is broader and shifted towards more negative values. Peak deconvolution yielded maxima at -12, -28 and -34 ppm, with an increase in intensity in the same order. Taking into account the regions for the mixed tetrahedra mentioned above, the same species as for PSZ appear to be present. As can be seen in Fig. 7 from the curves of the peak fit, the contribution of more nitrogen-rich tetrahedra is dominant in the 2DVB sample, whereas more carbon-rich tetrahedra appear dominant in the PSZ sample. These findings go along with the results of the elemental analysis, indicating that more nitrogen remains in the DVB containing samples, owing to the hindrance of nitrogen-eliminating reactions.

3.3.4. Raman spectroscopy

Raman spectroscopy yielded additional information about the free carbon phase after pyrolytic conversion at 600 °C (Fig. 8). Although NMR investigations after pyrolysis showed a small peak in the sp^2 carbon region for PSZ, no distinct signal can be detected by Raman, possibly a result from the relatively low signal-to-noise ratio. For 2DVB, in contrast, the *D* and *G* bands are clearly visible at 1358 cm^{-1} and 1584 cm^{-1}, respectively, clearly indicating carbon segregation at temperatures as low as 600 °C. Based on reports by Trassl et al. [56], it is

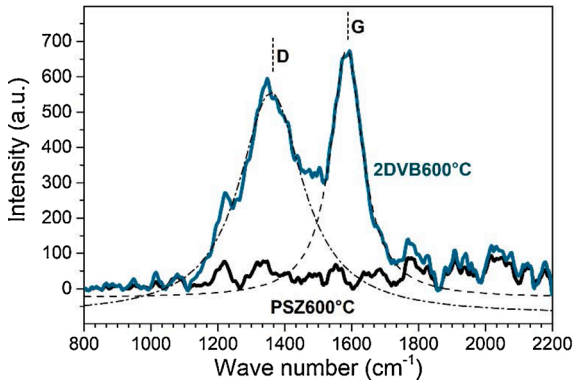

Fig. 8. Raman spectra of PSZ and 2DVB pyrolyzed at 600 °C; the dashed lines represent the fit of the D and G bands of the 2DVB material.

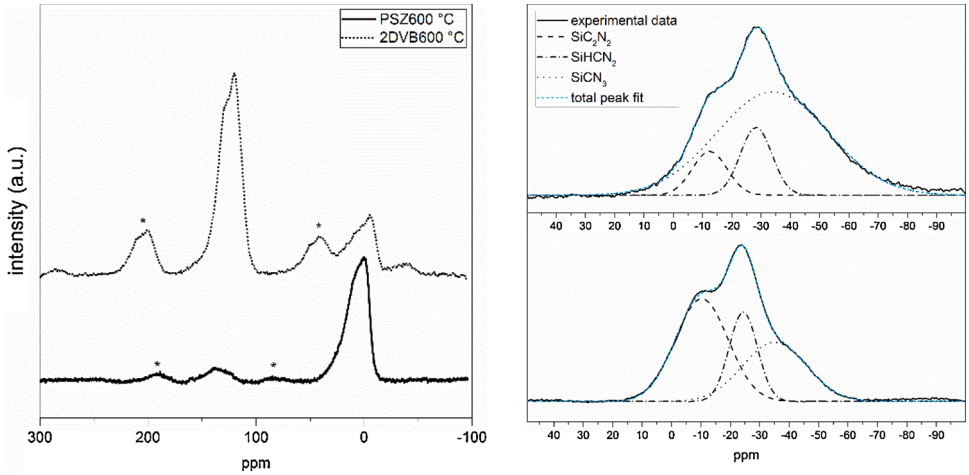

Fig. 7. ^{13}C (left) and ^{29}Si (right) solid state NMR spectra of PSZ (bottom) and 2DVB(top) pyrolyzed at 600 °C, together with the deconvoluted peaks of the ^{29}Si spectra.

possible to estimate the domain size of the carbon phase by using the integrated intensity ratio of the two bands, which in case of 2DVB yields a value of roughly 3 nm–5 nm. This domain size estimation underlines the conclusion that DVB molecules also react with each other and not only with PSZ oligomers during the crosslinking process.

3.3.5. Transmission Electron microscopy

For further elucidation of structural features, in particular the distribution of carbon, TEM investigations were carried out for both PSZ and 2DVB materials after pyrolytic conversion at 600 °C. Due to the amorphous nature and lack of phase contrast, no distinctions between the materials were visible in regular transmission electron micrographs (Fig. 9a and b), which is in accordance with reports by Chen et al. [49] who investigated PSZ-DVB-derived ceramics pyrolyzed at 1200 °C. However, by STEM-EELS and quantitative energy-filtering transmission electron microscopy (EFTEM) as described in detail by Hofer et al. [52], the presence of clusters with increased relative carbon concentration was found in 2DVB materials, whereas no distinct areas of increased carbon content are visible in PSZ materials (Fig. 9c and d). In combination with Raman data, these results suggest that carbon clusters in PSZ-DVB materials are already present at temperatures $\leq$ 600 °C.

3.4. Porosity in the amorphous SiCN(O) ceramics

As laid out in the previous sections, DVB shows a profound influence on the decomposition behaviour as well as on elemental composition and structural elements in the resulting ceramics. In order to determine whether these changes also affect the evolution of transient porosity during the polymer-to-ceramic conversion process, the resulting pore size of intermediate and final products was investigated in detail using two distinct methods, gas physisorption and small angle X-ray scattering (SAXS).

3.4.1. Gas physisorption

The porosity of the pyrolyzed materials was investigated using nitrogen gas physisorption at 77 K. The resulting isotherms and pore size distributions are shown in Fig. 10. The characteristics of the isotherms and the resulting porosity data are summarized in Table 2. In case of PSZ, the isotherms for materials pyrolyzed at 500 °C and 600 °C are typical Type I isotherms, with pyrolysis at 500 °C yielding the highest specific surface area. Pores appear to collapse at higher temperatures, eventually leading to a Type VI isotherm after pyrolysis at 700 °C, this being in accordance with previous investigations [31]. At the lowest investigated pyrolysis temperature, 400 °C, the shape of the isotherm is typical for a material which is non- or macroporous. This can either mean that the material is indeed non-porous, or that the pores are too small to be accessed by nitrogen physisorption, which is limited by the kinetic diameter of nitrogen (0.364 nm). The pore size distributions for the two samples yielding high specific surface areas and Type I isotherms, with pyrolysis temperatures of 500 °C and 600 °C, have their maxima at 0.88 nm and 0.84 nm, respectively. The maximum value for the sample pyrolyzed at 400 °C, the isotherm shape of which indicates a non- or macroporous sample, is 1.13 nm, but exhibiting a much lower micropore volume compared to the higher pyrolysis temperatures. For 2DVB, the sample pyrolyzed at 400 °C yields an isotherm typical for non- or macroporous samples, with the maximum of the pore size distribution at 1.13 nm as well. While the 2DVB sample pyrolyzed at 700 °C appears non-porous based on the shape of the isotherm, the samples pyrolyzed at 500 °C and 600 °C exhibit isotherms that are a mixture between Type I (microporous) and Type IV (mesoporous), the highest specific surface area found after pyrolysis at 500 °C. According to the pore size distribution, the size of mesopores is distributed over the whole mesopore range from 10 to 50 nm. However, mesopores only provide a minor contribution to the overall pore volume. The maximum of the pore size distribution of the 2DVB samples pyrolyzed at both 500 °C and 600 °C is 0.70 nm, but with lower micropore volume for the higher pyrolysis temperature. The isotherms for the 2DVB samples are comparable to isotherms of PSZ samples in terms of range and shape of the adsorption branch. However, an additional hysteresis loop (typical for a type IV isotherm) was observed for the samples pyrolyzed at 500 °C

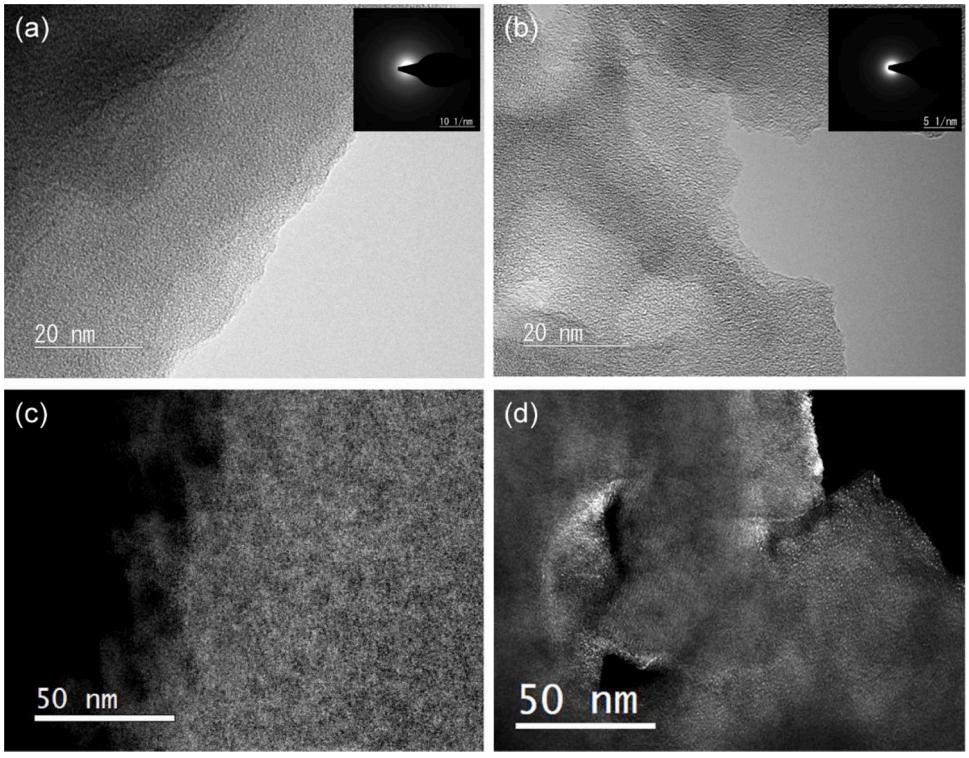

Fig. 9. TEM images of (a) PSZ and (b) 2DVB pyrolyzed at 600 °C, as well as (c, d) quantitative EFTEM maps of the same materials (c: PSZ; d: 2DVB) obtained by dividing the electron energy loss map of the Carbon K-edge with a thickness map (brighter areas indicate areas with increased relative carbon concentration).

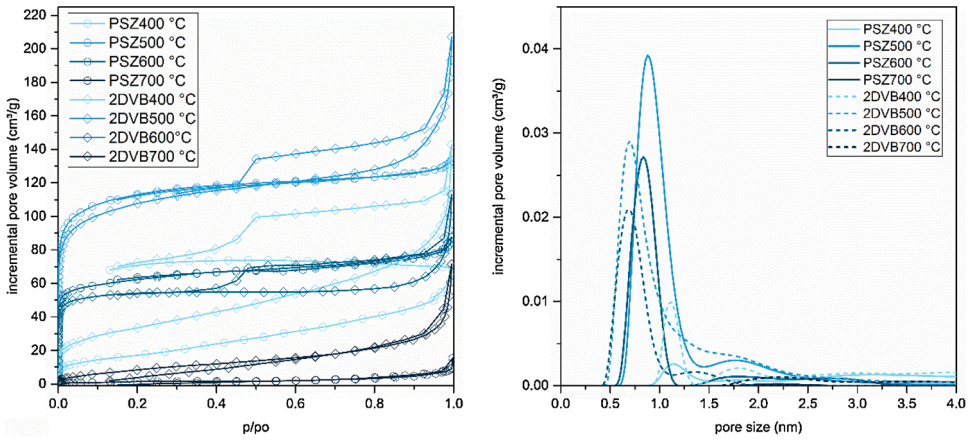

Fig. 10. Nitrogen gas physisorption isotherms and resulting pore size distributions of PSZ and 2DVB pyrolyzed at temperatures from 400 °C to 700 °C (pore size distributions calculated using NLDFT models).

Table 2
Type of isotherm, BET specific surface area (S_{BET}), maximum of the pore size distribution (PSD_{max}) in the micropore range, and micropore volume (V_{micro}) of PSZ and DVB pyrolyzed at temperatures between 400 and 700 °C (data from gas physisorption using N_2 at 77 K).

	Isotherm	S_{BET} (m^2/g)	PSD_{max} (nm)	V_{micro} (cm^3/g)	Comment
PSZ400 °C	Type II/VI	63 ± 1	1.13	0.02	Non- or macroporous
PSZ500 °C	Type I	350 ± 16	0.88	0.17	Microporous
PSZ600 °C	Type I	195 ± 6	0.84	0.10	Microporous
PSZ700 °C	Type VI	5 ± 0.5	–	–	Non porous
2DVB400 °C	Type II/VI	119 ± 1	1.13	0.02	Non- or macroporous
2DVB500 °C	Type I/IV	338 ± 14	0.70	0.16	Micro – and mesoporous
2DVB600 °C	Type I/IV	164 ± 9	0.70	0.08	Micro- and mesoporous
2DVB700 °C	Type VI	36 ± 1	–	–	Non porous

and 600 °C, indicating the presence of mesoporosity. The addition of DVB does not appear to significantly affect the temperature range of micropore stability, as both materials show the highest specific surface areas at 500 °C, and pores seem to collapse below 700 °C. Regarding the pore size, there is no difference between PSZ and 2DVB samples pyrolyzed at 400 °C. When comparing the samples pyrolyzed at 500 °C and 600 °C, a shift in the location of the pore size maximum can be observed depending on the initial composition. For 2DVB, the pore size maximum for both temperatures is located at 0.70 nm, in comparison to 0.84 nm for PSZ. The addition of an overstoichiometric amount of DVB therefore appears to influence the pore size both in the micropore and mesopore range if pyrolyzed in this temperature range.

3.4.2. Small-angle X-ray scattering (SAXS)

For more detailed investigations of the porosity, SAXS was selected as complimentary method. Experimental data are shown in Fig. 11, and the parameters calculated from the respective fitting procedure are listed in Table 3. The radii of gyration *Rg*, being considered as a measure for the size of micropores, appear to confirm the trends seen during physisorption studies. For PSZ, *2Rg* strongly increases from 400 °C to 500 °C (0.44 nm to 0.67 nm), where it seems to reach a plateau, with the value at 600 °C being comparable with 0.71 nm. At higher temperatures (700 °C, in this case), the pore size appears to decline again. All of the samples have a similar fractal dimension of around 4, which describes a sharp interface between bulk and pores, although the value is slightly lower in case of 400 °C compared to the other pyrolysis temperatures. The hard sphere radius, a measure for the distance between the

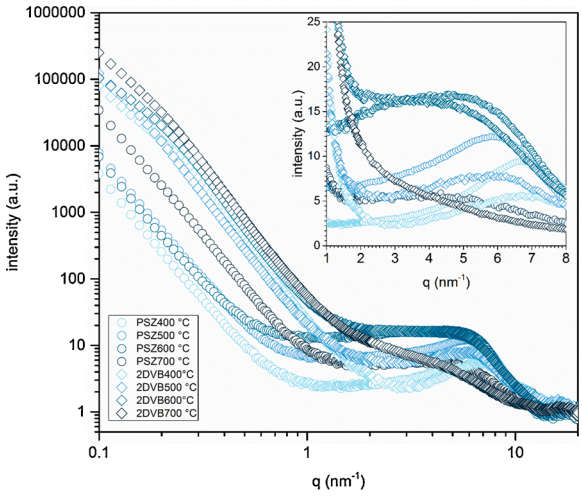

Fig. 11. Experimental SAXS curves of PSZ and 2DVB pyrolyzed at temperatures from 400 °C to 700 °C. The insert shows a section of the curves on a linear scale.

Table 3
Parameters obtained from applying a model fit to the SAXS data: Radius of gyration (R_g), fractal dimension (D), hard sphere radius (R_{hs}), and hard sphere volume fraction (η).

	$2R_g$ (nm)	D	$2R_{hs}$ (nm)	η
PSZ400 °C	0.44	3.5	0.44	0.12
PSZ500 °C	0.67	3.81	0.93	0.25
PSZ600 °C	0.71	3.85	0.89	0.19
PSZ700 °C	0.53	3.82	1.10	0.11
2DVB400 °C	0.42	4	0.86	0.42
2DVB500 °C	0.52	4	0.90	0.17
2DVB600 °C	0.48	4	–	–
2DVB700 °C	0.66	4	–	–

scattering objects (i.e., the pores), increases with increasing pyrolysis temperature, whereas the hard sphere volume ratio, a measure for the degree of agglomeration of pores, decreases for temperatures above 500 °C. This can be explained by pores evolving through decomposition of the organic groups, with pore growth and coarsening up to 600 °C, leading to larger pores with larger distance and a lower degree of agglomeration. Towards a temperature of 700 °C, the pores appear to collapse, as indicated by the smaller pore size and the lower amount of agglomeration (i.e., the lower hard sphere volume ratio). For 2DVB, *2Rg*

increases from 400 °C to 500 °C, and then again reaches a plateau. The fractal dimension is 4, which, again, stands for a sharp interface between bulk and pores. The spacing between the pores does not change significantly from 400 °C to 500 °C, and could not be determined for the higher temperatures. Agglomeration of pores significantly decreases from 400 °C to 500 °C. If the micropores are primarily located in the PSZ domains, which is likely since the pore size is in the range of that in the pure material, this could be explained by the partial decomposition of DVB in this temperature range, resulting in a more homogeneous distribution of the pores in the material.

For both PSZ and 2DVB, the pore characteristics as determined by SAXS are similar for 500 °C and 600 °C, but when comparing the two materials, there is a shift to smaller values for 2DVB, from 0.7 nm to 0.5 nm. Additionally, the radius of gyration is comparable for PSZ and 2DVB if the pyrolysis temperature is limited to 400 °C. However, the distance between the scattering centers (i.e., pores) is higher for 2DVB, which also exhibits a higher amount of agglomeration, as shown by the higher value of the hard sphere volume ratio η. These observations can be explained by the presence of DVB domains formed between PSZ oligomers. As micropores are most likely formed within PSZ, the spacing between the pores is larger, and they are less homogenously distributed due to being separated by DVB domains. Based on the observed radii of gyration, pore size in 2DVB materials appears to hardly change between 400 and 600 °C (showing a minor increase from 0.42 nm to 0.5 nm). In contrast, pore size in PSZ increases from 0.44 nm to 0.71 nm in the same temperature range. SAXS results show the presence of scattering centers after pyrolysis at 400 °C, even though physisorption isotherms of both PSZ and 2DVB only indicated a non- or macroporous material at this temperature. This discrepancy may be caused by the pore opening size at this temperature being too small to be accessed by nitrogen molecules during physisorption due to the kinetic diameter of nitrogen (0.364 nm).

4. Conclusions

A straightforward modification of the initial PSZ precursor network structure was successfully conducted through a hydrosilylation reaction using an overstoichiometric amount of DVB as linker, which was confirmed by elemental analysis as well as IR spectroscopy. The DVB molecules were shown to not only react with PSZ, but also with each other, leading to the evolution of DVB domains separating the PSZ oligomers from each other.

By investigation of the decomposition behaviour using TGA-MS, a strong influence of the linker on the occurring reactions was observed. Transamination reactions are drastically hindered below 450 °C, and the polymer-ceramic conversion is shifted to higher temperatures, which can be attributed to the prevented interactions between the oligomers until partial decomposition of DVB occurs. Elemental analysis showed an increase of the Si(+H)/N ratio for PSZ at increasing temperatures, whereas the Si(+H)/N ratio remained constant for 2DVB, illustrating a loss of nitrogen in case of PSZ while almost no nitrogen is lost during pyrolytic conversion in case of 2DVB. These findings were confirmed by ^{29}Si NMR of the samples at 600 °C, showing a higher contribution of nitrogen-rich mixed Si-C-N-tetrahedra in case of 2DVB. This effect can be explained by a hindering of transamination reactions leading to the loss of nitrogen by means of a release of ammonia. The ^{13}C spectra show the presence of sp^2 carbon for both PSZ and 2DVB, but to a higher extent in 2DVB as it stays integrated in the resulting ceramic. Raman and TEM results indeed showed the presence of, carbon-rich domains at temperatures $\leq$ 600 °C, consequently leading to a free C phase.

The pore size of samples was significantly affected by the introduction of DVB into the base precursor compound, as shown by gas physisorption and SAXS investigations. While no difference between linker-free and linker-containing samples was found after pyrolysis at 400 °C, a shift to smaller pore sizes was observed at higher pyrolysis temperatures in case of 2DVB. According to N_2 physisorption, PSD_{max} shifts from 0.88 and 0.84 nm at 400 °C to 0.70 nm for 500 °C and 600 °C. SAXS investigations confirm this trend, with $2R_g$ decreasing from ~0.7 nm to ~0.5 nm. After heat treatment at 700 °C, microporosity disappears both in presence and absence of the linker compound.

Based on these observations, the introduction of DVB into poly(vinyl)silazane appears to shift the size of microporosity without drastically influencing the thermal stability of pores. Although no direct increase in thermal stability of pores was observed, a clear difference in decomposition behaviour of the preceramic polymer and a change in pore size were found. As transamination reactions are hindered, the nitrogen content of the final material therefore is higher than in the absence of DVB. The shift in pore size is most likely an indirect effect of the DVB due to the change in composition of the micropore-forming entities. Consequently, this strengthens the hypothesis that the composition of the micropore-forming entities is one of the deciding factors in determining the final pore size in polymer-derived ceramic materials. This represents an essential finding, acting as basis for future work aimed towards tailoring of the resulting pore size towards specific application-dependent requirements.

Declaration of Competing Interest

The authors report no declarations of interest.

Acknowledgements

Funding of this work by the Austrian Science Fund (FWF): P29058 is gratefully acknowledged. The authors thank Karin Wieland for her support in Raman characterization.

Appendix A. Supplementary data

Supplementary material related to this article can be found, in the online version, at doi:https://doi.org/10.1016/j.jeurceramsoc.2021.01.051.

References

[1] M. Thommes, K. Kaneko, A.V. Neimark, J.P. Olivier, F. Rodriguez-Reinoso, J. Rouquerol, et al., Physisorption of gases, with special reference to the evaluation of surface area and pore size distribution (IUPAC Technical Report), Pure Appl. Chem. 87 (2015) 1051–1069.
[2] A.J. Burggraaf, L. Cot, Fundamentals of Inorganic Membrane Science and Technology, Elsevier, 1996.
[3] Y. Seishi, H. Josaburo, O. Mamoru, Continuous silicon carbide fiber of high tensile strength, Chem. Lett. 4 (1975) 931–934.
[4] P. Colombo, G. Mera, R. Riedel, G.D. Sorarù, Polymer-derived ceramics: 40 years of research and innovation in advanced ceramics, J. Am. Ceram. Soc. 93 (2010) 1805–1837.
[5] C. Vakifahmetoglu, D. Zeydanli, P. Colombo, Porous polymer derived ceramics, Mater. Sci. Eng. R Rep. 106 (2016) 1–30.
[6] A. Viard, D. Fonblanc, D. Lopez-Ferber, M. Schmidt, A. Lale, C. Durif, et al., Polymer derived Si–B–C–N ceramics: 30 years of research, Adv. Eng. Mater. (2018) 20.
[7] R. Riedel, G. Mera, R. Hauser, A. Klonczynski, Silicon-based polymer-derived ceramics: synthesis properties and applications - a review, Nippon Seramikkusu Kyokai Gakujutsu Ronbunshi/J. Ceramic Soci. Japn. 114 (2006) 425–444.
[8] M. Schulz, Polymer derived ceramics in MEMS/NEMS – a review on production processes and application, Adv. Appl. Ceram. 108 (2009) 454–460.
[9] M. Günthner, T. Kraus, A. Dierdorf, D. Decker, W. Krenkel, G. Motz, Advanced coatings on the basis of Si(C)N precursors for protection of steel against oxidation, J. Eur. Ceram. Soc. 29 (2009) 2061–2068.
[10] S. Sarkar, L. Zhai, Polymer-derived non-oxide ceramic fibers—Past, present and future, Mater. Express 1 (2011) 18–29.
[11] R.M. Prasad, A. Gurlo, R. Riedel, M. Hübner, N. Barsan, U. Weimar, Microporous ceramic coated SnO2 sensors for hydrogen and carbon monoxide sensing in harsh reducing conditions, Sens. Actuators B Chem. 149 (2010) 105–109.
[12] A. Viard, P. Miele, S. Bernard, Polymer-derived ceramics route toward SiCN and SiBCN fibers: from chemistry of polycarbosilazanes to the design and characterization of ceramic fibers, J. Ceram Soc. Jpn. 124 (2016) 967–980.
[13] G. Barroso, Q. Li, R.K. Bordia, G. Motz, Polymeric and ceramic silicon-based coatings – a review, J. Mater. Chem. A 7 (2019) 1936–1963.
[14] H. Yang, P. Deschatelets, S.T. Brittain, G.M. Whitesides, Fabrication of high performance ceramic microstructures from a polymeric precursor using Soft lithography, Adv. Mater. 13 (2001) 54–58.

[15] L.-A. Liew, Y. Liu, R. Luo, T. Cross, L. An, V.M. Bright, et al., Fabrication of SiCN MEMS by photopolymerization of pre-ceramic polymer, Sens. Actuators A Phys. 95 (2002) 120–134.
[16] L.-A. Liew, W. Zhang, V.M. Bright, L. An, M.L. Dunn, R. Raj, Fabrication of SiCN ceramic MEMS using injectable polymer-precursor technique, Sens. Actuators A Phys. 89 (2001) 64–70.
[17] J. Grossenbacher, M.R. Gullo, V. Bakumov, G. Blugan, J. Kuebler, J. Brugger, On the micrometre precise mould filling of liquid polymer derived ceramic precursor for 300-mm-thick high aspect ratio ceramic MEMS, Ceram. Int. 41 (2015) 623–629.
[18] P. Colombo, E. Bernardo, Macro- and micro-cellular porous ceramics from preceramic polymers, Compos. Sci. Technol. 63 (2003) 2353–2359.
[19] P. Colombo, J.R. Hellmann, Ceramic foams from preceramic polymers, Mater. Res. Innov. 6 (2002) 260–272.
[20] A. Lale, M. Schmidt, M.D. Mallmann, A.V.A. Bezerra, E.D. Acosta, R.A.F. Machado, et al., Polymer-Derived Ceramics with engineered mesoporosity: from design to application in catalysis, Surf. Coat. Technol. 350 (2018) 569–586.
[21] L. Biasetto, Functional Ceramic Foams From Preceramic Polymers, Università di Bologna, Dipartimento di Chimica Applicata e Scienza dei Materiali, Dissertation, 2007.
[22] Y. Iwamoto, Precursors-derived ceramic membranes for high-temperature separation of hydrogen, J. Ceram Soc. Jpn. 115 (2007) 947–954.
[23] R.M. Prasad, Polymer-Derived Microporous Ceramics for Membranes and Sensors for High Temperature Hydrogen Purification and Sensing. TU Darmstadt, PhD Thesis, 2012.
[24] Y. Jüttke, H. Richter, I. Voigt, R.M. Prasad, M.S. Bazarjani, A. Gurlo, et al., Polymer derived ceramic membranes for gas separation, Chem. Eng. Trans. 32 (2013) 1891–1896.
[25] J.P. Dismukes, J.W. Johnson, J.S. Bradley, J.M. Millar, Chemical synthesis of microporous nonoxide ceramics from Polysilazanes, Chem. Mater. 9 (1997) 699–706.
[26] H.M. Williams, E.A. Dawson, P.A. Barnes, B. Rand, R.M.D. Brydson, A.R. Brough, High temperature ceramics for use in membrane reactors: the development of microporosity during the pyrolysis of polycarbosilanes, J. Mater. Chem. 12 (2002) 3754–3760.
[27] A.R. Maddocks, D.J. Cassidy, A.S. Jones, A.T. Harris, Synthesis of nanoporous silicon carbide via the preceramic polymer route, Mater. Chem. Phys. 113 (2009) 861–867.
[28] M. Seifollahi Bazarjani, H.-J. Kleebe, M.M. Müller, C. Fasel, M. Baghaie Yazdi, A. Gurlo, et al., Nanoporous silicon oxycarbonitride ceramics derived from polysilazanes in situ modified with nickel nanoparticles, Chem. Mater. 23 (2011) 4112–4123.
[29] C. Schitco, M.S. Bazarjani, R. Riedel, A. Gurlo, NH3-assisted synthesis of microporous silicon oxycarbonitride ceramics from preceramic polymers: a combined N2 and CO2 adsorption and small angle X-ray scattering study, J. Mater. Chem. A 3 (2015) 805–818.
[30] C. Schiţco, C. Turdean-Ionescu, M.S. Bazarjani, C.-W. Tai, D. Li, C. Fasel, et al., Silicon oxycarbonitrides synthesized by ammonia-assisted thermolysis route from polymers: A total X-ray scattering, solid.-state NMR, and TEM structural study, J. Eur. Ceram. Soc. 36 (2016) 979–989.
[31] T. Konegger, C.-C. Tsai, H. Peterlik, S.E. Creager, R.K. Bordia, Asymmetric polysilazane-derived ceramic structures with multiscalar porosity for membrane applications, Microporous Mesoporous Mater. 232 (2016) 196–204.
[32] J.S. Bradley, O. Vollmer, R. Rovai, U. Specht, F. Lefebvre, High surface area silicon imidonitrides: a new class of microporous solid base, Adv. Mater. 10 (1998) 938–942.
[33] M. Seifollahi Bazarjani, M.M. Müller, H.-J. Kleebe, Y. Jüttke, I. Voigt, M. Baghaie Yazdi, et al., High-Temperature Stability and Saturation Magnetization of Superparamagnetic Nickel Nanoparticles in Microporous Polysilazane-Derived Ceramics and their Gas Permeation Properties, ACS Appl. Mater. Interfaces 6 (2014) 12270–12278.
[34] M. Zaheer, C.D. Keenan, J. Hermannsdörfer, E. Roessler, G. Motz, J. Senker, et al., Robust microporous monoliths with integrated catalytically active metal sites investigated by hyperpolarized 129Xe NMR, Chem. Mater. 24 (2012) 3952–3963.
[35] Q. Wen, Y. Xu, B. Xu, C. Fasel, O. Guillon, G. Buntkowsky, et al., Single-source-precursor synthesis of dense SiC/HfCxN1-x-based ultrahigh-temperature ceramic nanocomposites, Nanoscale 6 (2014) 13678–13689.
[36] R.J.P. Corriu, D. Leclercq, P.H. Mutin, J.M. Planeix, A. Vioux, Mechanism of pyrolysis of polycarbosilanes: poly(silylethylene) and poly(dimethylsilylethylene), Organometallics 12 (1993) 454–462.
[37] D. Bahloul, M. Pereira, C. Gerardin, Pyrolysis chemistry of polysilazane precursors to silicon carbonitride, J. Mater. Chem. 7 (1997) 109–116.
[38] T. Breuning, Study of pyrolysis of polysilazane precursor in Si□C□(O,N) system, J. Anal. Appl. Pyrolysis 49 (1999) 43–51.
[39] Y. Li, E. Kroke, R. Riedel, C. Fasel, C. Gervais, F. Babonneau, Thermal cross-linking and pyrolytic conversion of poly(ureamethylvinyl)silazanes to silicon-based ceramics, Appl. Organomet. Chem. 15 (2001) 820–832.
[40] H. Suda, H. Yamauchi, Y. Uchimaru, I. Fujiwara, K. Haraya, Structural evolution during conversion of polycarbosilane precursor into silicon carbide-based microporous membranes, J. Ceram Soc. Jpn. 114 (2006) 539–544.
[41] W. Chen, J. Zhou, Study on the pyrolysis behavior of polycarbosilane, J. Wuhan Univ. Technol. Sci. Ed. 30 (2015) 679–683.
[42] E. Kroke, Y.L. Li, C. Konetschny, E. Lecomte, C. Fasel, R. Riedel, Silazane derived ceramics and related materials, Mater. Sci. Eng. R Rep. 26 (2000) 197–199.
[43] A.R. Maddocks, J.M. Hook, H. Stender, A.T. Harris, Heterogeneously catalysed crosslinking of polycarbosilane with divinylbenzene, J. Mater. Sci. 43 (2008) 2666–2674.
[44] G. Liu, J. Kaspar, L.M. Reinold, M. Graczyk-Zajac, R. Riedel, Electrochemical performance of DVB-modified SiOC and SiCN polymer-derived negative electrodes for lithium-ion batteries, Electrochim. Acta 106 (2013) 101–108.
[45] P. Vallachira Warriam Sasikumar, E. Zera, M. Graczyk-Zajac, R. Riedel, G. D. Soraru, Structural design of polymer-derived SiOC ceramic aerogels for high-rate Li ion storage applications, J. Am. Ceram. Soc. 99 (2016) 2977–2983.
[46] B. Ma, Y. Cao, Y. Gao, Y. Wang, Fabrication of a thin double-layer thermistor based on DVB-modified polymer-derived SiCN ceramics, J. Alloys. Compd. 732 (2018) 491–497.
[47] F. Dalcanale, J. Grossenbacher, G. Blugan, M.R. Gullo, A. Lauria, J. Brugger, et al., Influence of carbon enrichment on electrical conductivity and processing of polycarbosilane derived ceramic for MEMS applications, J. Eur. Ceram. Soc. 34 (2014) 3559–3570.
[48] Y. Iwamoto, W. Völger, E. Kroke, R. Riedel, T. Saitou, K. Matsunaga, Crystallization behavior of amorphous silicon carbonitride ceramics derived from organometallic precursors, J. Am. Ceram. Soc. 84 (2001) 2170–2178.
[49] Y. Chen, C. Li, Y. Wang, Q. Zhang, C. Xu, B. Wei, et al., Self-assembled carbon–silicon carbonitride nanocomposites: high-performance anode materials for lithium-ion batteries, J. Mater. Chem. 21 (2011) 18186–18190.
[50] G. Beaucage, D.W. Schaefer, Structural studies of complex systems using small-angle scattering: a unified Guinier/power-law approach, J. Non. Solids 172-174 (1994) 797–805.
[51] D.J. Kinning, E.L. Thomas, Hard-sphere interactions between spherical domains in diblock copolymers, Macromolecules 17 (1984) 1712–1718.
[52] F. Hofer, W. Grogger, P. Warbichler, I. Papst, Quantitative energy-filtering transmission electron microscopy (EFTEM), Microchim. Acta 132 (2000) 273–288.
[53] C. Gérardin, F. Taulelle, D. Bahloul, Pyrolysis chemistry of polysilazane precursors to silicon carbonitride: part 2. - Solid-state NMR of the pyrolytic residues, J. Mater. Chem. 7 (1997) 117–126.
[54] J.D. Kenneth, M.E.S. MacKenzie, Multinuclear Solid-state Nuclear Magnetic Resonance of Inorganic Materials, Pergamon materials series, 2002.
[55] Q. Zhang, Z. Yang, D. Jia, Q. Chen, Y. Zhou, Synthesis and structural evolution of dual-boron-source-modified polysilazane derived SiBCN ceramics, New J. Chem. 40 (2016) 7034–7042.
[56] S. Trassl, G. Motz, E. Rössler, G. Ziegler, Characterization of the free-carbon phase in precursor-derived Si-C-N ceramics: I, spectroscopic methods, J. Am. Ceram. Soc. 85 (2002) 239–244.